Version of Record: https://www.sciencedirect.com/science/article/pii/S0029549317300997
Manuscript_69b549f05f7cfbf5cc37c1067238108d

Extreme earthquake response of nuclear power plants isolated using sliding bearings

Manish Kumar[a,*], Andrew S. Whittaker[b], Michael C. Constantinou[b]

[a]*Department of Civil Engineering, Indian Institute of Technology Gandhinagar, Gandhinagar, India, 382355; formerly graduate student at University at Buffalo, Buffalo, NY, 14260*
[b]*Department of Civil, Structural and Environmental Engineering, University at Buffalo, Buffalo, NY, 14260*

Abstract

Horizontal seismic isolation is a viable approach to mitigate risk to structures, systems and components (SSCs) in nuclear power plants (NPPs) under extreme ground shaking. This paper presents a study on an NPP seismically isolated using single concave Friction Pendulum™ (FP) bearings subjected to ground motions representing seismic hazard at two US sites: Diablo Canyon and Vogtle. Two models of the NPP, five models to describe friction at the sliding surface of the FP bearings, and four levels of ground shaking are considered for response-history analysis, which provide insight into the influence of 1) the required level of detail of an NPP model, 2) the vertical component of ground motion on response of isolated NPPs, and 3) the pressure-, temperature- and/or velocity-dependencies of the coefficient of friction, on the response of an isolated NPP. The isolation-system displacement of an NPP can be estimated using a macro model subjected to only the two orthogonal horizontal components of ground motion. The variation of the coefficient of friction with temperature at the sliding surface during earthquake shaking should be accounted for in the calculation of isolation-system displacements, particularly when the shaking intensity is high; pressure and velocity dependencies are not important. In-structure floor spectra should be computed using a detailed three-dimensional model of an isolated NPP subjected to all three components of ground motion.

Keywords: nuclear power plants, auxiliary and shield building, containment internal structure, seismic isolation, Friction Pendulum™, temperature-dependence of friction

1. Introduction

Nuclear power plants (NPPs) are designed for severe internal and external natural and man-made hazards, including earthquakes. Extreme earthquakes can challenge new and existing NPPs, with large forces expected in internal structures, systems and components (SSCs) under design basis shaking. Base isolation is a viable strategy to seismically protect SSCs in NPPs, since it effectively filters a significant fraction of the high-frequency horizontal earthquake shaking, and facilitates standardization of plant designs (e.g., Huang et al. (2007, 2010, 2011a,b), Kumar et al. (2017)). Sliding isolators, here single concave Friction Pendulum™ (FP) bearings, are one type of hardware that could be used in the United States for safety-related nuclear structures, including NPPs (see Kammerer et al. (forthcoming)).

This paper presents the results of response-history analyses of an NPP seismically isolated using FP bearings. The sample NPP includes three major structures: auxiliary and shield building (ASB), containment internal structure (CIS) and steel containment vessel (SCV). The ASB considered herein is a 140,000-ton concrete structure with a footprint of 97 m × 60 m, and a total height of 89 m (Roche, 2013). The CIS weighs 41,000 tons with a total height of 33 m (Short et al., 2007). The SCV weighs 3,700 tons and is ignored in this study due to its relatively small mass (see Short et al. (2007)). Two models of the sample NPP are developed. The first model of the NPP is the ASB and CIS supported on a common isolation system comprising single-concave FP bearings. The second model of the NPP involves a macro (single) FP bearing with aggregated properties of the Model 1 isolation system. Friction at the

*Corresponding author
Email address: mkumar@iitgn.ac.in (Manish Kumar)

sliding surface is described by the five models proposed by Kumar et al. (2015a), which update, time step by time step, the coefficient of friction at the sliding surface of a bearing as a function of the axial pressure on the bearing, horizontal velocity of the slider relative to the sliding surface, and/or temperature at the sliding surface.

Results are reported here for analysis of the two NPP models subjected to four intensities of ground motion shaking: 1) design basis earthquake (DBE) shaking at the site of the Diablo Canyon Nuclear Generating Station (DCNGS), 2) beyond design basis earthquake shaking at the site of the DCNGS as defined in ASCE/SEI Standard 4-16 (ASCE, 2016), 3) beyond design basis earthquake shaking at the site of the DCNGS as defined in the draft seismic isolation NUREG (Kammerer et al., forthcoming), and 4) beyond design basis earthquake shaking at the site of the Vogtle Electric Generating Plant (or Plant Vogtle) as defined in the draft seismic isolation NUREG (Kammerer et al., forthcoming). Displacements and in-structure spectral demands for DBE shaking at the site of the Vogtle Electric Generating Plant are (relatively) small and are not reported here; see Kumar et al. (2015b) for information.

The site of the DCNGS, on the coast in Southern California (latitude: 35.2116 N, longitude: 120.8556 W) is associated with high seismic hazard. The site of the Plant Vogtle, in Waynesboro, Georgia (latitude: 33.1433 N, longitude: 81.7606 W) is associated with moderate seismic hazard. These two sites span the range of seismic hazard that might be considered appropriate for the seismic isolation of a large light water reactor in the United States (see Section 2).

Two definitions of beyond design basis earthquake (BDBE) shaking are addressed here. The first is adopted from ASCE/SEI Standard 43-05 (ASCE, 2005) and ASCE/SEI Standard 4-16, namely, the intensity of BDBE shaking is 150% of the intensity (or amplitude) of DBE shaking. The second is that presented in the draft seismic isolation NUREG, namely, the intensity of BDBE shaking is described by uniform hazard spectra with a mean annual frequency of exceedance of 10^{-5}. (The draft NUREG requires the amplitude of BDBE spectra to be no less than 167% of the amplitude of the DBE spectra, but that does not control for sites studied by the authors in the United States.) The same definition of design basis earthquake shaking is used in ASCE/SEI Standards 43-05 and 4-16, and the draft seismic isolation NUREG for design of seismic isolation systems, namely, uniform hazard spectra with a mean annual frequency of exceedance of 10^{-4}.

Model 1 of the NPP is subjected to a) the two horizontal components of ground motions only, and b) all three components, whereas Model 2 is subjected only to the two horizontal components. Two response quantities are studied, namely, isolation-system displacements, and floor spectral ordinates at different locations in the CIS. The study helps answer the following questions: 1) can the response of an NPP be estimated for preliminary design and assessment using a simplified model of the NPP? 2) how does the definition of friction at the sliding surface of the FP bearings influence response?, and 3) how important is it to include the vertical component of ground motions in the response-history analyses?

2. Geometric properties of the nuclear power plant

2.1. Auxiliary and shield building (ASB)

Figures 1 and 2 present plan and elevation views of the ASB, respectively. The dimensions of the ASB were provided by Roche (Roche, 2013). The ASB is 97 m $\times$ 60 m in plan and its height is 89 m measured from the bottom of the basemat. The interior walls, floors and roof are 0.6 m (2 ft) thick. The exterior walls and the walls along the horizontal axes of symmetry are 0.9 m (3 ft) thick. The ASB is constructed of reinforced concrete with a density of 2,400 kg/m^3, a characteristic concrete strength of 41.3 MPa and an elastic modulus of 30.4 GPa. The total mass of the ASB is 140,000 ton, with the 49,000 ton in the basemat, which is shown stippled in Figure 2.

2.2. Containment internal structure (CIS)

The CIS is modeled as a vertical stick with masses lumped at different heights and at three outrigger nodes. Figure 3 is a schematic of the 33 m-tall CIS. The circles indicate the locations of concentrated mass. The total mass of CIS is 41,000 ton. The CIS model used in this study is from Short et al. (2007). This model was developed by Short et al. to study the effects of soil-structure interaction and seismic wave incoherence. The details on the mass and stiffness properties of the CIS model are presented in Kumar et al. (2015b).

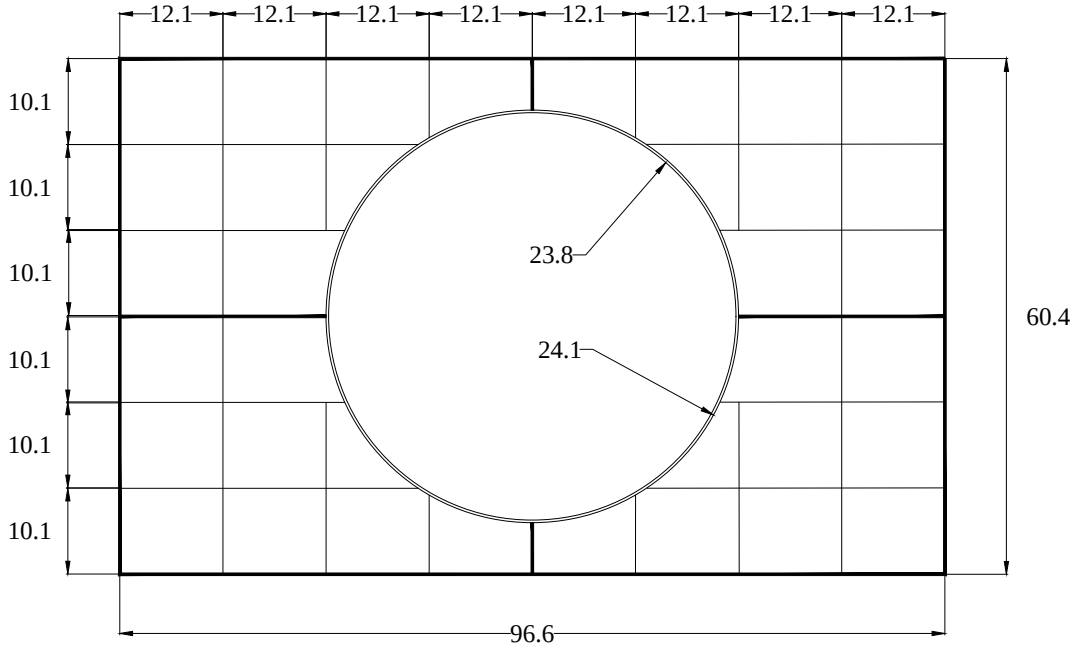

- Dimensions are in meters.
- Exterior walls and the walls along the central lines are 0.9 m (3 ft) thick.
- Interior walls are 0.6 m (2 ft) thick.
- The circle of radius 24.1 m (80 ft) indicates the 1.2 m (4 ft) thick cylindrical wall.
- The circle of radius 23.8 m (79 ft) indicates the 0.9 m (3 ft) thick hemispherical dome.

Figure 1: Plan view of auxiliary and shield building (adapted from Roche (2013))

3. Modeling ASB and CIS for response-history analysis

3.1. Introduction

This section summarizes the approach used to model the ASB for response-history analysis using OpenSees (PEER, 2014). The distribution of the mass of the walls, floors, roof, cylindrical wall and hemispherical dome, and of the lateral stiffness contributed by the walls, cylinder and dome are discussed. The mass associated with the nodes and the stiffness of the elements used in the OpenSees model are identified. The dynamic properties (e.g., natural period and corresponding mode shape) of the ASB modelled in OpenSees are computed and compared with those obtained for the ASB modeled in LS-DYNA (LSTC, 2011), where the LS-DYNA model for the ASB was provided by Roche (2013).

The containment internal structure is modeled in OpenSees using the mass and stiffness data presented in Short et al. (2007).

3.2. Auxiliary and shield building (ASB)

3.2.1. LS-DYNA model

The auxiliary and shield building with plan and elevation views shown in Figures 1 and 2, was modeled in LS-DYNA by Roche (2013). Figure 4 shows the model of the ASB. The concrete characteristic strength was 41.3 MPa and its elastic modulus was 30.4 GPa.

The natural periods for the first two modes of vibration of the ASB modeled using LS-DYNA are listed in Table 1. The first two mode shapes are shown in Figure 5.

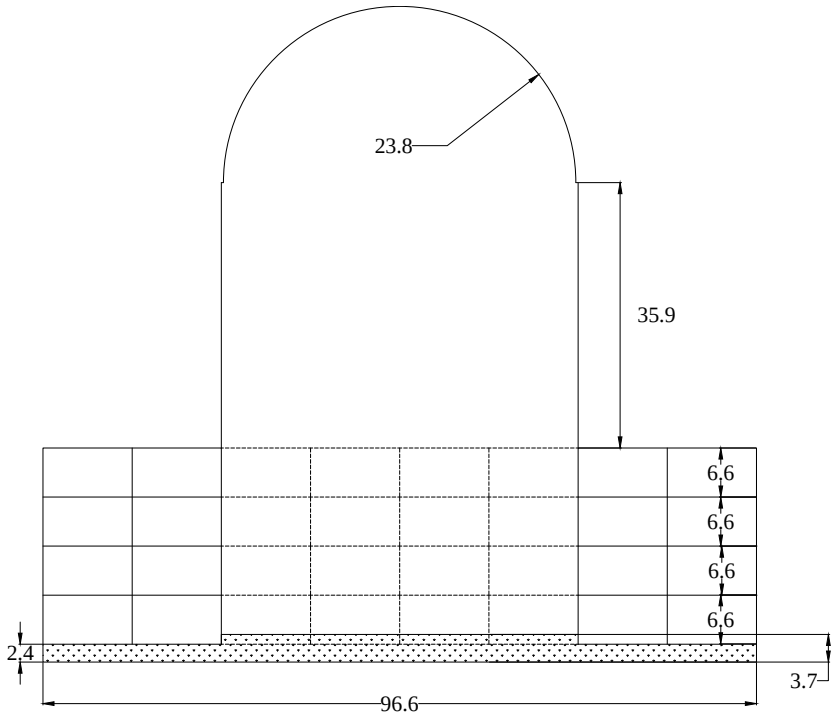

- Dimensions are in meters.
- Floors and roof are 0.6 m (2 ft) thick.
- Thickness of cylindrical wall is 1.2 m (4 ft).
- Thickness of hemispherical dome is 0.9 m (3 ft).

Figure 2: Elevation view of auxiliary and shield building (adapted from Roche (2013))

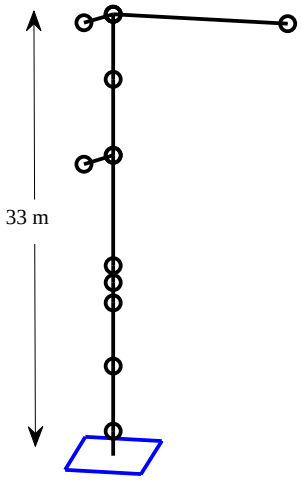

Figure 3: Containment internal structure (adapted from Short et al. (2007))

3.2.2. OpenSees model

The auxiliary and shield building is divided into three segments to facilitate modeling in OpenSees. The three segments are shown in Figure 6. Segment 2 is the central portion of the ASB comprising the cylindrical wall and its dome, with plan dimensions of 48 m $\times$ 60 m. Segments 1 and 3 are symmetrically placed with respect to Segment 2;

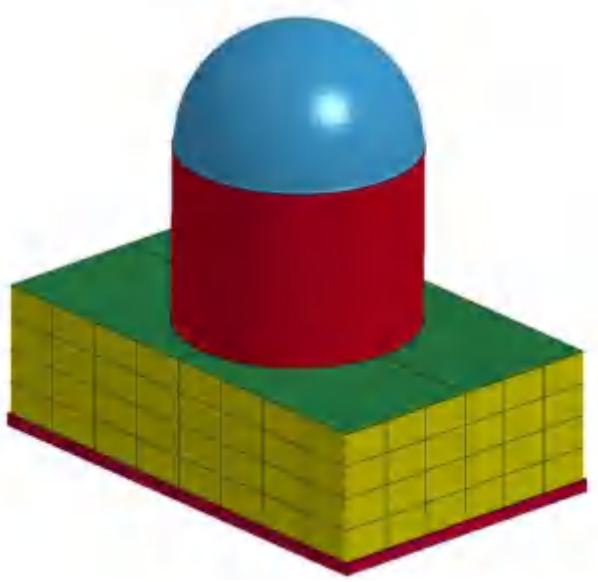

Figure 4: LS-DYNA model of the ASB (adapted from Roche (2013))

Table 1: Natural periods of the ASB

Mode	LS-DYNA	OpenSees
1	0.23 s	0.15 s
2	0.22 s	0.15 s

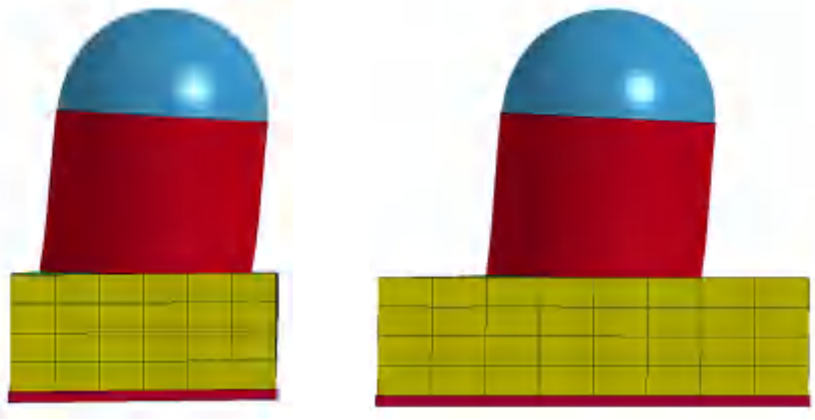

(a) First mode (b) Second mode

Figure 5: Mode shapes of the ASB obtained using LS-DYNA

each has plan dimensions of 24 m × 60 m.

Segment 1 of the ASB comprises a 2.4 m-thick basemat and four floors (including the roof), each 0.6 m-thick. The total length of 0.9 m-thick external walls, 0.9 m-thick internal walls and 0.6 m-thick internal walls is 109 m, 24 m and 198 m, respectively. The story height is 6.6 m.

Five elevations are considered in Segment 1, namely, 1.2 m, 9.1 m, 15.8 m, 22.6 m and 29.3 m, which represent

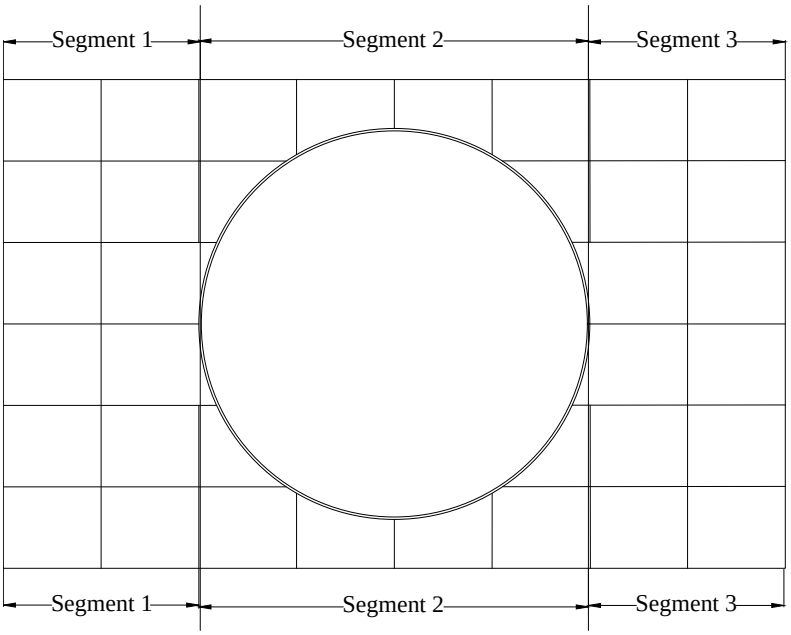

Figure 6: Segments of auxiliary and shield building (ASB)

the locations of the basemat and the floors. Masses are lumped at the floors and the basemat. The mass of each wall is split between the floors above and below. The mass at each level is listed in Table 2.

Table 2: Distribution of mass in the ASB

Level	**Height from bottom of basemat (m)**	**Mass (tonnes)**		
		Segment 1	Segment 2	Segment 3
1	1.2	11,000	27,000	11,000
2	9.1	5,800	6,700	5,800
3	15.8	5,800	7,000	5,800
4	22.6	5,800	7,000	5,800
5	29.3	4,000	6,600	4,000
6	41.5	-	5,300	-
7	53.6	-	5,300	-
8	65.8	-	3,800	-
9	71.3	-	6,700	-
	Total	32,000	75,000	32,000

Segment 2 of the ASB comprises 1) a 1.2 m-thick cylindrical wall with a radius and a height of 24 m and 62 m, respectively, 2) a 0.9 m-thick hemisphere with a radius of 24 m, 3) 0.9 m-thick exterior walls with a total length 97 m, 4) 0.9 m-thick interior walls with a total length of 12 m, 5) 0.6 m-thick interior walls with a total length of 89 m, 6) a 2.4 m-thick basemat with plan dimensions of 48 m $\times$ 60 m, 7) a 1.3 m-thick circular basemat on top of the rectangular basemat with a radius of 24 m, and 8) 0.6 m-thick floors at four levels (same as Segments 1 and 3) with a plan area of 1,100 m^2. In addition to the five elevations considered for Segments 1 and 3, four elevations, at heights of 41.5 m, 53.6 m, 65.8 m and 71.3 m measured from the bottom of the basemat, are considered for Segment 2. Mass is assigned to levels per the method adopted for Segments 1 and 3. The mass at the nine elevations of Segment 2 are listed in Table 2.

The mass associated with an elevation in a segment is distributed across nodes that are equispaced in plan. For this study, the spacing between nodes is 6 m for all three segments of the ASB. Consequently, there are 187 nodes at each of the five elevations lower than 30 m, and 99 nodes at each of the four higher elevations: a total of 1,331 nodes (5×187+4×99) for the ASB. Figures 7 and 8 present the locations of the nodes in plan and elevation, respectively.

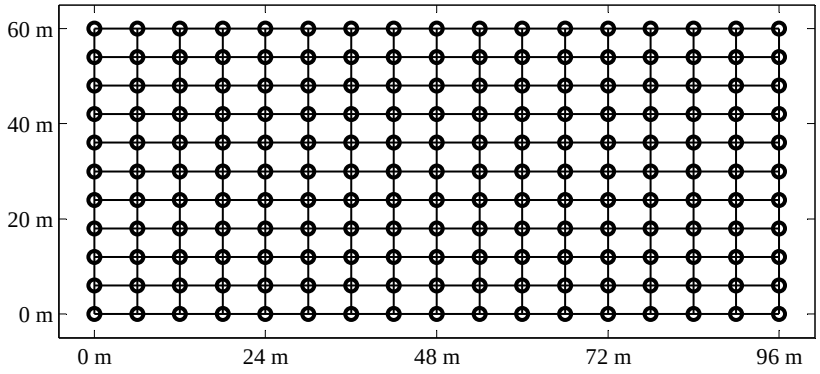

(a) Levels 1 through 5

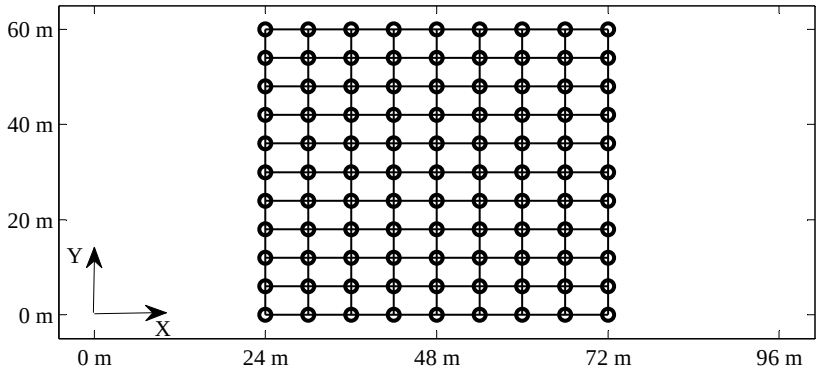

(b) Levels 6 through 9

Figure 7: Locations of nodes (indicated by circles) in the ASB in plan

A small value of mass moment of inertia is assigned about the three axes to all 1,331 nodes in the OpenSees model of the ASB to avoid numerical instability. The locations of nodes, and the masses and mass moments of inertia associated with the nodes are listed in Appendix I of Kumar et al. (2015b). The 1,331 nodes are connected through discrete beam-column elements, details of which are presented in Chapter 8 and Appendix I of Kumar et al. (2015b).

3.2.2.1. Dynamic properties. Table 1 lists the first two natural periods of the LS-DYNA and OpenSees models. The OpenSees mode shapes are plotted in Figure 9. The first translational mode is in the short direction (60 m, see Figure 1) of the ASB; the second translational mode is in the long direction. The OpenSees and LS-DYNA natural periods and mode shapes are similar, enabling the OpenSees model to be used to answer the three questions posed in Section 1.

3.3. Containment internal structure (CIS)

The containment internal structure (CIS) is modeled in OpenSees as a vertical stick with three outrigger nodes (see Figure 3). This fixed-base CIS model is identical to that of Short et al. (2007). The CIS model responds dynamically in the vertical and horizontal directions, but only the horizontal dynamic response is studied in this paper because the

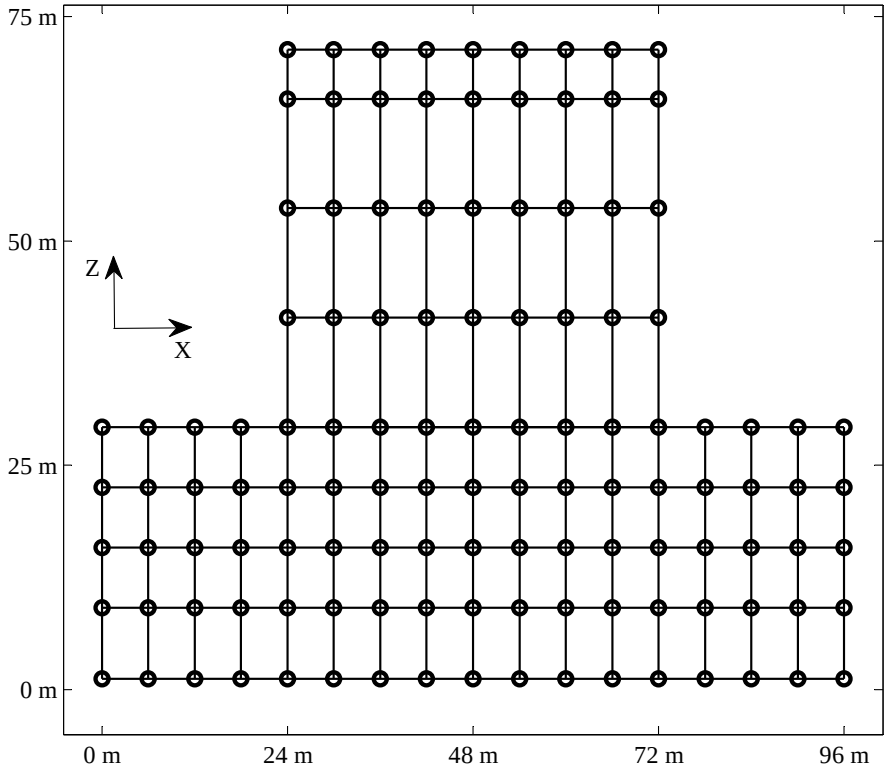

Figure 8: Locations of nodes (indicated by circles) in the ASB in elevation

inertial effects of the vertical mass of the CIS accumulate at the node at the center of the basemat (see Figure 7(a), and Kumar et al. (2015b)) leading to unrealistically high vertical inertial forces. Details of the CIS model developed in OpenSees are presented in Kumar et al. (2015b).

The natural periods of the CIS associated with the motion in the horizontal directions are listed in Table 3. These periods compare favorably with the values reported in Short et al. (2007).

Table 3: Natural periods of containment internal structure

	Period (s)	
Mode	Present study	Short et al. (2007)
1	0.082	0.083
2	0.078	0.075
3	0.061	0.067
4	0.053	0.057
5	0.048	0.050
6	0.042	0.035

4. Description of the seismically isolated models of the NPP

Two models of a seismically isolated nuclear power plant, one more detailed than the other, are analyzed to compute isolation-system displacements and horizontal floor spectra for nodes at different locations in the CIS.

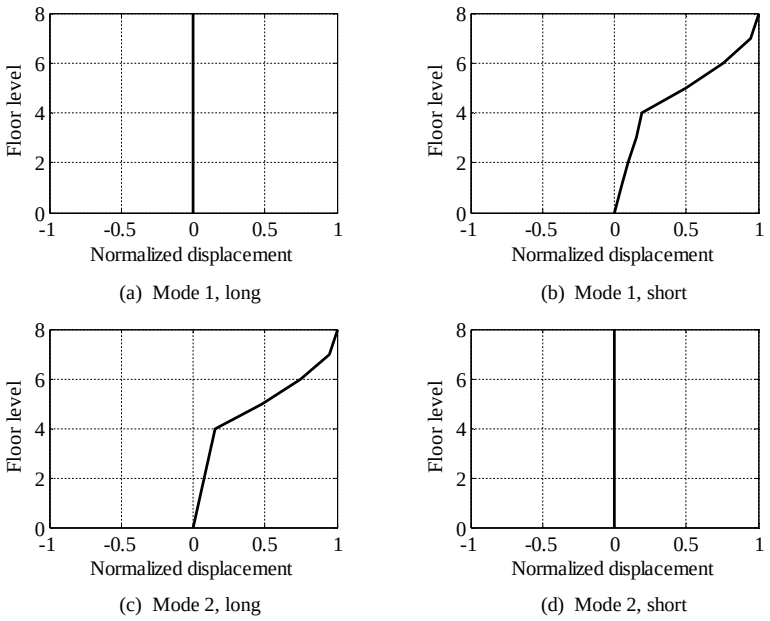

Figure 9: Mode shapes corresponding to the first two natural periods of vibration of the ASB

Two percent Rayleigh damping is assigned at periods of 0.05 s and 3 s[1]. The displacement at which sliding commences is set equal to 1 mm (e.g., Constantinou et al. (2007), Kumar et al. (2015a)).

4.1. Model 1: seismically isolated ASB and CIS

The ASB model comprises 187 nodes at the basemat level; the base of the CIS is represented by one node. One node (109060) is common to both the ASB and the CIS. One hundred eighty seven single FP bearings are used to isolate the ASB and CIS. Each of the bottommost 187 nodes (height = 1.2 m; see Table 2 and Figure 7(a)) of the common basemat represents the slider of an FP bearing. One hundred eighty seven additional nodes, each of which represents the sliding surface of an FP bearing, are introduced at the plan locations of the bottommost 187 nodes of the ASB. The nodes representing the sliding surface are restrained from translation and rotation; the nodes representing the slider are free to translate but restrained from rotation (a boundary condition enforced by the stiff basemat).

Gravity and inertial forces associated with the entire mass of the CIS are transferred at node 109060, which represents the slider of the FP bearing at the geometrical center of the basemat. The axial force on this bearing, and consequently the shear force and horizontal floor spectral ordinates, would be unrealistically high. The gravity force due to the CIS is therefore distributed equally among all 99 nodes of Segment 2 of the ASB (see Figure 6) representing sliders of FP bearings. The vertical inertial mass of the CIS is ignored in this study.

4.1.1. Seismic isolation system

The seismic isolation system comprises 187 single FP bearings with a sliding period of 3 s, reference coefficient of friction[2] of 0.06, static axial pressure of 50 MPa and friction at the sliding surface defined using the five friction models listed in Table 4: see Kumar et al. (2015a) for further details. The center-to-center distance between adjacent bearings is 6 m. The bearings are placed at the nodes shown in Figure 7(a). The static axial load on each FP bearing in Segments 1 and 3 (see Figure 6) is 7,100 kN (32,000 tons distributed between 44 bearings; see Table 2). The

[1]The range covers the dominant natural periods of the CIS (see Table 3) and the sliding period of the FP bearings.

[2]The coefficient of friction at the sliding surface of an FP bearing measured at the static axial pressure, a high velocity (e.g., 1 m/s) and a sliding-surface temperature of 20°C (Kumar et al., 2015a).

static axial load on the bearings in Segment 2 is 11,000 kN (75,000 tons from the ASB and 41,000 tons from the CIS, distributed between 99 bearings). The radius of the contact area for each of the 44 FP bearings in Segments 1 and 3 is 0.21 m, and 0.26 m for each of the 99 FP bearings in Segment 2. The resulting static axial pressure on each of the 187 bearings of the isolation system is 50 MPa.

Table 4: Isolator friction models (see Kumar et al. (2015a))

Model	Description
1	Coulomb
2	Pressure-dependent
3	Temperature-dependent
4	Velocity-dependent
5	Pressure-, temperature- and velocity-dependent

4.2. Model 2: macro model (single FP bearing)

Model 2 is a macro model of the NPP comprising a single FP bearing and a lumped mass to describe the superstructure. A sliding period of 3 s, reference coefficient of friction of 0.06, static axial pressure of 50 MPa and friction at the sliding surface defined using the five models of Table 4 are considered. The static axial load on the bearing is the weighted average[3] of the static axial loads on the 187 FP bearings of Model 1: 9,200 kN. The radius of the contact area at the sliding surface is 0.24 m. The inertial masses associated with motion in the three translational directions are equal to the gravity load.

5. Ground motions for response-history analyses

Per Section 1, Models 1 and 2 are subjected to four intensities of ground motion, all derived from DBE ground motions (hazard with a mean annual frequency of 10^{-4}) for the site of the DCNGS. Amplitude scale factors are listed in Table 5, together with descriptions of the site and level of shaking. Sections 5.1 and 5.2 present the bases for the DBE and BDBE (per the draft seismic isolation NUREG) scale factors for the DCNGS, respectively. Section 5.3 presents the basis for BDBE scale factor for Plant Vogtle. Plant Vogtle information is presented here because results for the scale factor of 0.6 are provided in Section 6.

Table 5: Amplitude scaling factors to represent seismic hazard at different sites

Amplitude scaling factor	Description
0.6	BDBE shaking at Plant Vogtle per draft seismic isolation NUREG
1.0	DBE shaking at DCNGS per draft seismic isolation NUREG
1.5	BDBE shaking at DCNGS per ASCE 4-16
2.0	BDBE shaking at DCNGS per draft seismic isolation NUREG

5.1. DBE shaking at DCNGS

Figure 10(a) presents the uniform hazard response spectrum (UHRS) in the horizontal direction for the site of the DCNGS and a return period of 10,000 years (data obtained from the USGS website http://geohazards.usgs.gov/hazardtool/application.php; accessed on July 15, 2014). The response spectra of the X component of the 30 seeds motions listed in Table 6 spectrally matched to the UHRS are also plotted in Figure 10(a). The period range considered for spectral matching is 0.01 s to 5 s. Figure 10(b) provides similar information in the orthogonal horizontal direction Y.

[3]The static axial force on each of the 44 FP bearings of the seismically isolated ASB-CIS (Section 4.1) in Segments 1 and 3 is 7,100 kN. The force on each of the 99 bearings in Segment 2 of this model is 11,000 kN.

The UHRS in the two orthogonal directions are identical[4]. The response spectra of the matched motions compare well with the target UHRS in both the principal horizontal directions.

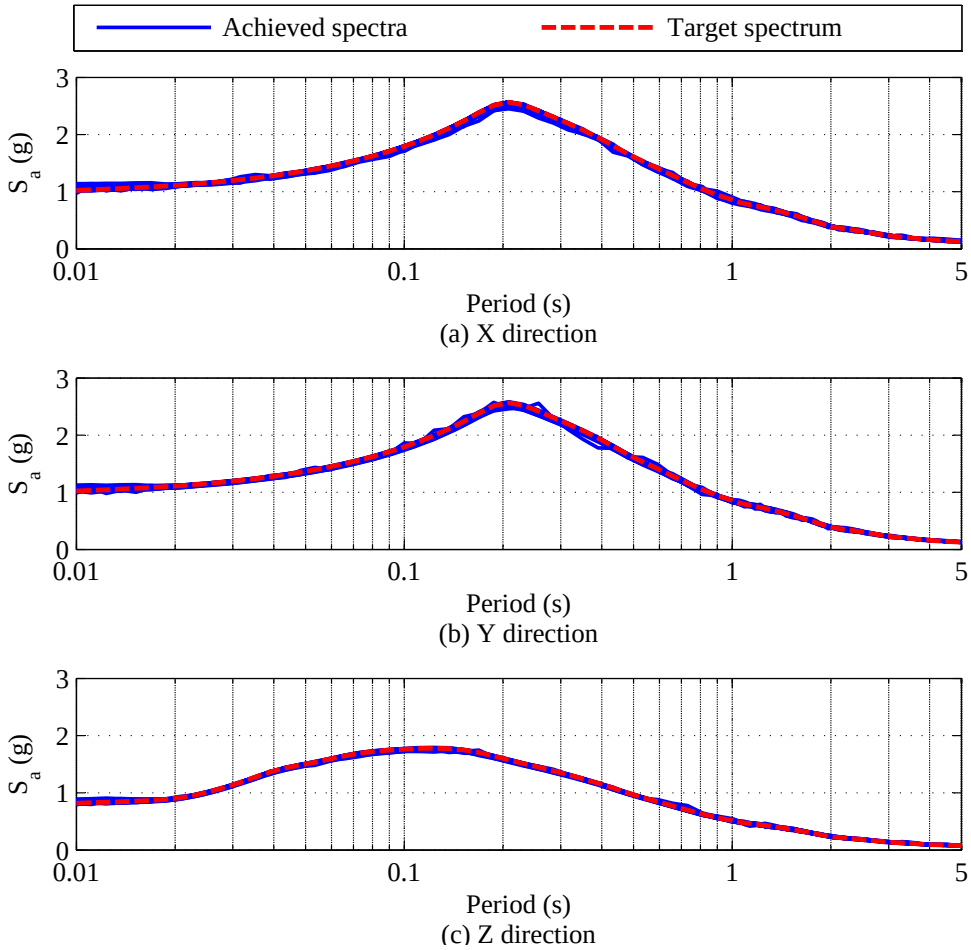

Figure 10: Response spectra of the ground motions spectrally matched to the 10,000-year UHRS for the DCNGS

The target spectrum in the vertical direction is obtained by multiplying the UHRS of Figure 10(a) (and 10(b)) with the ratio of vertical to horizontal (V-H ratios) spectra of Figure 11. These ratios are obtained based on the information presented in Gülerce and Abrahamson (2011) (also see Kumar et al. (2015b)). The UHRS in the vertical direction, and the response spectra of the Z (vertical) component of the seed motions matched to the vertical UHRS are plotted in Figure 10(c).

5.2. BDBE shaking at DCNGS

The draft seismic isolation NUREG defines BDBE shaking using UHRS with a mean annual frequency of exceedance of 10^{-5} (return period of 100,000 years). The 100,000-year UHRS for horizontal shaking is also obtained from the USGS website. The ratios of the 100,000-year to 10,000-year spectral ordinates at selected natural periods are plotted in Figure 12, which range between 1.8 and 1.9 for periods less than 1 s, and between 1.9 and 2.1 at

[4]Differences between the amplitudes of the two orthogonal horizontal components of ground motions should be accounted for: Max-min per Huang et al. (2009, 2013).

Table 6: Seed motions spectrally matched to the 10,000-year UHRS for the Diablo Canyon site

Sl No	NGA Number	Event	Year	Magnitude	Epicentral distance (km)
1	72	San Fernando	1971	6.6	24
2	77	San Fernando	1971	6.6	12
3	80	San Fernando	1971	6.6	39
4	180	Imperial Valley	1979	6.5	28
5	284	Irpinia	1980	6.9	33
6	285	Irpinia	1980	6.9	23
7	68	San Fernando	1971	6.6	40
8	292	Irpinia	1980	6.9	30
9	763	Loma Prieta	1989	6.9	29
10	179	Imperial Valley	1979	6.5	27
11	161	Imperial Valley	1979	6.5	43
12	810	Loma Prieta	1989	6.9	16
13	184	Imperial Valley	1979	6.5	27
14	957	Northridge	1994	6.7	64
15	1107	Kobe	1995	6.9	24
16	994	Northridge	1994	6.7	25
17	1011	Northridge	1994	6.7	19
18	1012	Northridge	1994	6.7	14
19	1021	Northridge	1994	6.7	50
20	1050	Northridge	1994	6.7	20
21	1051	Northridge	1994	6.7	20
22	1078	Northridge	1994	6.7	15
23	1091	Northridge	1994	6.7	38
24	1528	Chi-Chi	1999	7.6	45
25	159	Imperial Valley	1979	6.5	3
26	879	Landers	1992	7.3	44
27	754	Loma Prieta	1989	6.9	31
28	802	Loma Prieta	1989	6.9	27
29	1633	Manjil	1990	7.4	40
30	1144	Gulf of Aqaba	1995	7.2	93

longer periods. The 10,000-year ground motions for DCNGS (see Figure 10), amplitude scaled by a factor of 2.0, are used here to represent 100,000-year shaking at the site. A discussion on the appropriateness of amplitude scaling the ground motions is presented in Appendix G of Kumar et al. (2015b).

5.3. BDBE shaking at Plant Vogtle

The 10,000-year (DBE) and 100,000-year (BDBE) UHRS for the site of the Vogtle nuclear power plant (latitude: 33.1433 N, longitude: 81.7606 W) are obtained from the USGS website identified previously; the assumed shear wave velocity in the upper 30 m of the soil column is 760 m/sec. The ratio of the 10,000-year UHRS ordinates for Plant Vogtle to DCNGS ranges between 0.2 and 0.3 for periods between 0.01 s and 2 s. The ratio of the Plant Vogtle 100,000-year UHRS ordinates to the DCNGS 10,000-year UHRS ordinates ranges between 0.5 and 0.9 at period less than 1 s, and between 0.5 and 0.7 at longer periods. Figure 13 presents the DBE and BDBE ratios as a function of period. Herein, an amplitude scale factor of 0.6 is used to generate Plant Vogtle BDBE ground motions for response-history analysis from the DCNGS DBE motions. Kumar et al. (2015b) presents additional information for the site of Plant Vogtle.

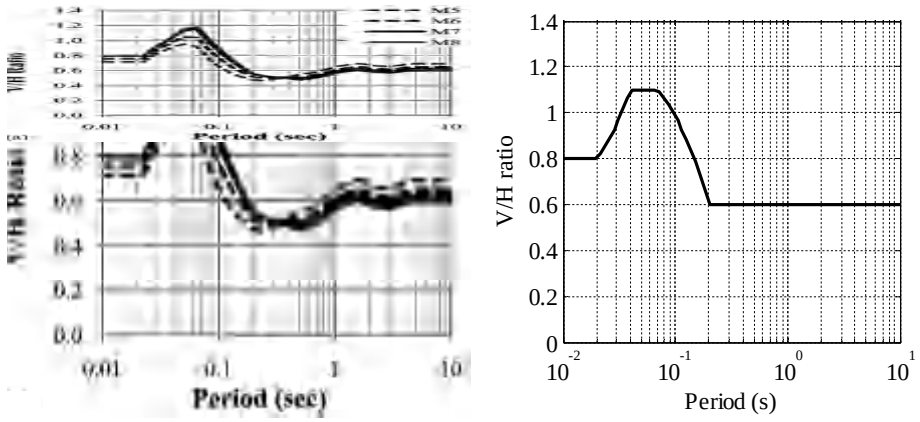

(a) Gülerce and Abrahamson (2011)

(b) V/H versus period ratio assumed in this study

Figure 11: Median ratio of vertical to horizontal spectral response on a rock site with a source-to-site distance of 5 km (see Gülerce and Abrahamson (2011) and Kumar et al. (2015b))

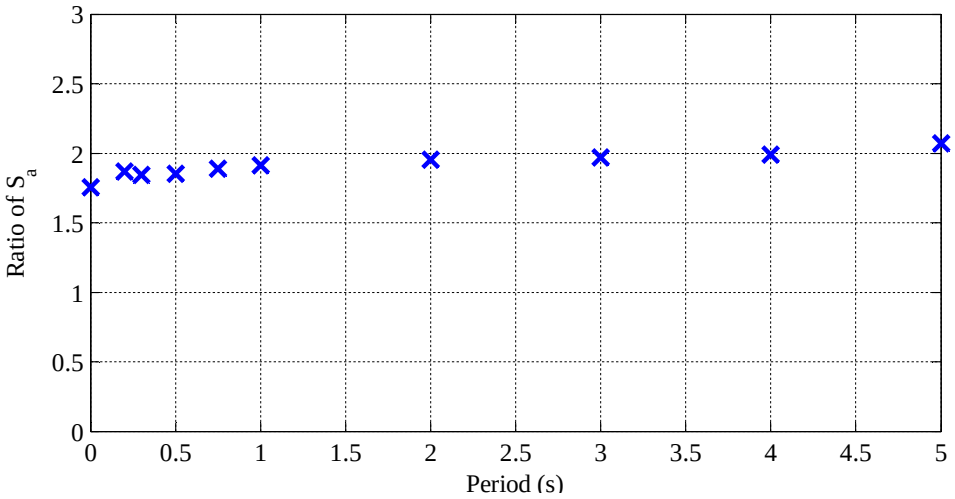

Figure 12: Ratio of horizontal UHRS ordinates for 100,000 years to 10,000 years at the DCNGS

6. Results

This section presents results of the response-history analyses performed on the two NPP models subjected to the four sets of 30 ground motions with a focus on the amplitude scaling factor of 0.6; results for other three scaling factors are summarized in this paper and presented in detail in Kumar et al. (2015b). Model 1 is subjected to a) three components of ground motion, and b) two horizontal components of ground motions; Model 2 of the NPP is subjected to the two horizontal components only to help answer the questions posed in Section 1. Distributions of peak isolation-system displacements and floor spectral accelerations are presented and studied. Table 7 maps the computed response quantities to the models.

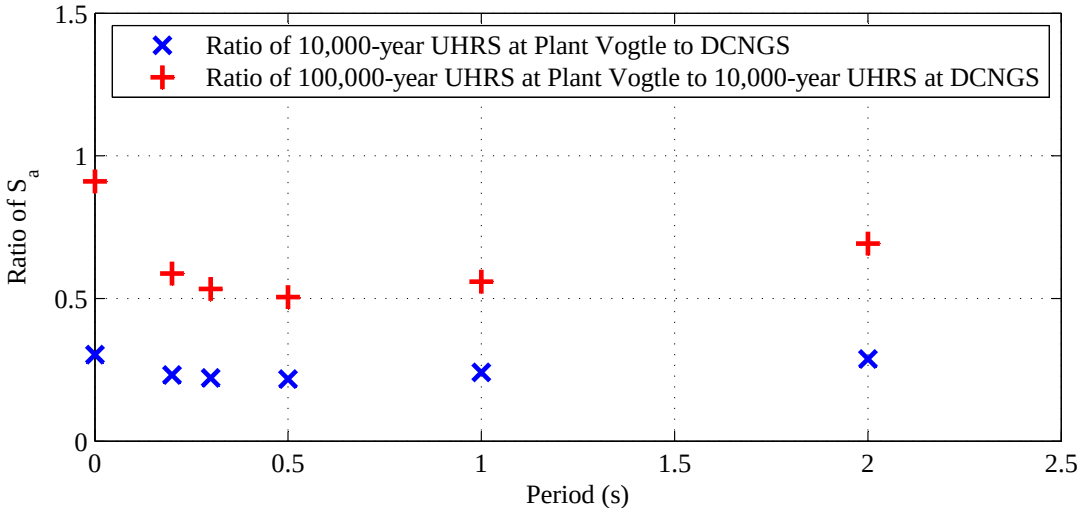

Figure 13: Ratio of horizontal UHRS ordinates for 10,000-year and 100,000-year at Plant Vogtle to 10,000-year ordinates at DCNGS

Table 7: Response quantities estimated using the two models

Model	**Description**	**Response quantity**		
		Isolation-system displacement	Acceleration of basemat	Acceleration of nodes of CIS
1	Isolated ASB-CIS	✓	✓	✓
2	Macro model	✓	✓	×

6.1. Distribution of peak displacements

Figure 14(a) presents the distributions of displacements of the center of the isolation system for Models 1 and 2, with friction at the sliding surface of FP bearings described using the Coulomb model, subjected to the set of 30 ground motions of Figure 10 amplitude scaled by 0.6. Model 1 is subjected to ground motions with and without the vertical component. The distributions of the isolation-system displacements obtained using the two models are virtually identical, with a less than 2 mm (5 mm) difference in the median (99th percentile) displacement. This observation is identical to that of Mosqueda et al. (2004). Including the vertical component of the ground motion in the response-history analysis of Model 1 alters the median (99th percentile) isolation system displacement estimate by 0.1 mm (1 mm).

Figures 14(b) through 14(e) present results for Model 1 and Model 2, with friction at the sliding surface described using the pressure-dependent, temperature-dependent, velocity-dependent, and *p-T-v* model, respectively. The distributions of the isolation-system displacements computed using the two NPP models do not differ materially. The displacements of panels (a), (b) and (d) are virtually identical, implying that the pressure- and velocity-dependencies of coefficient of friction do not affect the calculation of peak displacements. These displacements are smaller than those in panels (c) and (e), wherein heating effects are accounted for. Results for the scaling factor of 1.0, 1.5 and 2.0 are presented in Kumar et al. (2015b). The distributions of isolation-system displacements are similar, for a given intensity level and friction model.

6.1.1. Influence of definition of friction at the sliding surface

Large cyclic changes in the coefficient of friction are observed during the course of an analysis for bearings at different locations, when friction at the sliding surface is defined using the pressure-dependent model. Consider the seismically isolated ASB-CIS model (Model 1) with a reference coefficient of friction of 0.06 and friction at the sliding surface described using the pressure-dependent friction model subjected to the two horizontal and vertical components of ground motion 1 (GM1) of Figure 10 (see also Table 6) with an amplitude scale factor of 1.0. The coefficient of

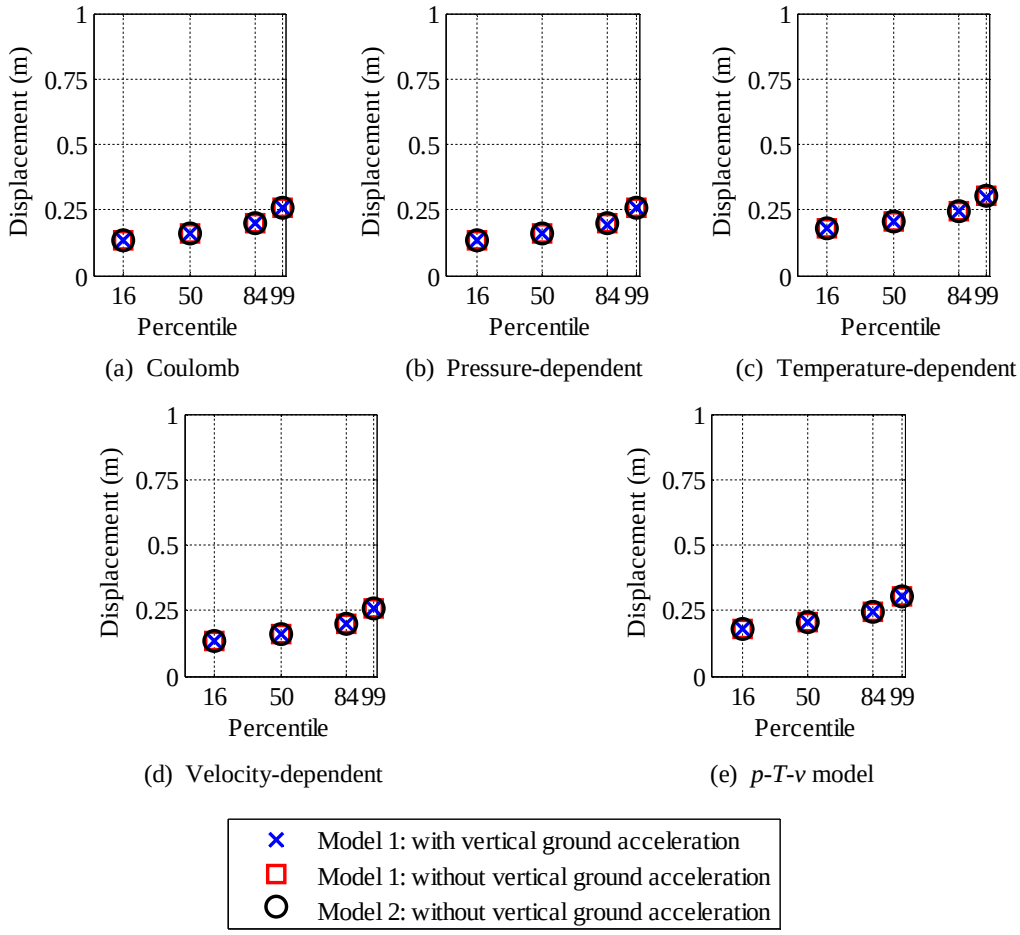

Figure 14: Distributions of isolation-system displacement for the three models subjected to the set of ground motions amplitude scaled by 0.6

friction at the sliding surface of the bearing at a corner of the isolation system varies between 0.046 and 0.082[5] during the course of shaking, and that at the center of the isolation system varies between 0.052 and 0.071. When the isolated ASB-CIS model is subjected only to the horizontal components of GM1, the coefficient varies between 0.051 and 0.069 for the bearing at the corner, and between 0.060 and 0.060 for the bearing at the center of the isolation system. These changes[6] in the coefficient of friction do not alter the distribution of isolation-system displacement[7] relative to that calculated ignoring the pressure-dependence of friction.

The calculated displacements do not change materially if the velocity-dependence of the coefficient of friction is considered in the analysis, which is expected since the coefficient of friction is essentially constant at the high velocities expected during *strong* shaking (see Constantinou et al. (2007)).

Inclusion of temperature-dependency in the friction model significantly changes the estimate of isolation-system displacement, as noted previously. The coefficient of friction reduces to about half the reference value during *strong* shaking, which leads to a greater isolation-system displacement. The influence of heating on displacements, which

[5]The coefficient of friction increases with decreasing axial pressure. The axial pressure on a bearing at a given location in the isolation system changes over the course of earthquake shaking due to the vertical component of ground motion and the response of the supported superstructure to the three components of ground motion (see Kumar et al. (2015b)).

[6]The average coefficient of friction for a bearing is 0.06 over the course of shaking, irrespective of location.

[7]The median (99th percentile) displacements for Coulomb and pressure-dependent friction models differ by less than 0.5 mm.

is a function of shaking intensity, static axial pressure and reference coefficient of friction, is discussed in detail in Kumar et al. (2015b)[8].

6.2. Floor response spectra

Floor spectra at the nodes 109060 (basemat level), 532 (height of 13 m), 5351 (height of 24 m) and 5382 (height of 34 m) of the CIS (see Kumar et al. (2015b)) are computed using the two NPP models with friction at the sliding surface of the FP bearings defined using the five models of Table 4 subjected to the set of 30 ground motions developed in Section 5.1 amplitude scaled by 0.6, 1.0, 1.5 and 2.0. This section presents a portion of these results; the remaining results can be found in Kumar et al. (2015b).

Figure 15(a) presents the median floor spectrum in the X direction at node 109060 obtained using Model 1 with friction at the sliding surface of the FP bearings described using Coulomb model subjected to the two horizontal and vertical components of the 30 ground motions of Figure 10 amplitude scaled by 0.6. The results for Model 1 subjected to the 30 sets of three-components ground motions are referred to as *benchmark* results in this section. Also plotted in the figure are the floor spectra for Models 1 and 2 subjected to only two horizontal components of the ground motions. The floor spectral ordinates at 0.01 s at node 109060 (basemat) corresponding to the two NPP models subjected to the horizontal components of the ground motions only are smaller than the *benchmark* results by 7% and 20%, respectively. These differences are 12% and 44% at 0.05 s, 3% and 18% at 0.1 s, and 1% and 3% at 1 s. Therefore, all three components of motion are needed to generate horizontal floor spectra.

Figures 15(d) through 15(l) present the 50^{th}, 90^{th} and 99^{th} percentile floor response spectra at nodes 532, 5351 and 5382 of the CIS, computed using Model 1. The general observations are similar to those for node 109060. The floor spectra for the velocity-dependent, temperature-dependent, pressure-dependent and *p-T-v* friction models are presented in Figures 16 through 19, respectively. The spectra for the ground motion amplitude scaling factors of 1.0 (DBE at DCNGS per the draft isolation NUREG), 1.5 (BDBE at DCNGS per ASCE 4-16) and 2.0 (BDBE at DCNGS per the draft isolation NUREG) are presented in Kumar et al. (2015b). Observations on the calculation of spectral ordinates are summarized below.

i. The horizontal spectral ordinates computed using Model 1 subjected to the two horizontal components of ground motions are considerably smaller than those obtained for the model subjected to all three components of ground motions.

ii. The differences between the *benchmark* horizontal ordinates and those calculated for the two models subjected to the two horizontal components of ground motions only:

   (a) increase substantially with increasing shaking intensity at periods 0.01 s, 0.05 s and 0.1 s (see Figure 20)

   (b) are small at 1 s irrespective of shaking intensity (see Figure 20)

   (c) are greater at the higher percentiles

   (d) are generally greater for nodes at higher elevations inside containment

iii. The choice of friction model does not considerably influence the floor spectral ordinates, especially for the nodes close to the basemat (see Figure 21).

7. Summary and conclusions

This paper presents the results of the response-history analyses performed on an NPP subjected to ground motions representing hazard at the sites of Diablo Canyon and Vogtle—sites of high and moderate seismic hazard, respectively. Two models of an NPP, five models to define friction at the sliding surface of the single concave FP bearings, and sets of 30 ground motions consistent with 1) DBE shaking at the DCNGS, 2) BDBE shaking at the DCNGS (two definitions), and 3) BDBE shaking at Plant Vogtle are considered in this study. The structural system, internal equipment

[8]This observation is specific to the single concave FP bearing. The effect of heating will be significantly smaller if the triple concave FP bearing (e.g., Fenz and Constantinou (2008)) is used instead because energy is dissipated via friction and heat on multiple sliding surfaces.

and the isolation system are explicitly modeled in the first model of the NPP, whereas a macro bearing is considered to represent the isolated NPP in the second model. Five friction models are used to update the coefficient of friction at the sliding surface of FP bearings with axial pressure, temperature at the sliding surface and/or sliding velocity during the course of earthquake shaking.

The following conclusions are drawn on the modeling, analysis and design of an NPP isolated with single concave FP bearings:

i. Isolation-system horizontal displacement can be estimated for preliminary design using a macro model of the isolation system (e.g., a single FP bearing) subjected to the two horizontal components of the ground motions.

ii. The friction model used to compute isolation-system displacement should address heating effects. Displacements may be significantly underestimated otherwise, especially for high intensity shaking.

iii. The friction model need not consider the velocity- and pressure-dependence of the coefficient of friction to compute isolation-system displacement.

iv. Floor spectra in isolated nuclear structures should be computed using a detailed 3D finite element model of the isolated superstructure. The vertical component of ground motion must be included to compute horizontal floor spectra. The choice of friction model does not significantly influence the floor spectral ordinates, particularly at lower elevations in containment.

Acknowledgement

The financial support provided through a grant to MCEER and the University at Buffalo from the United State Nuclear Regulatory Commission and the Lawrence Berkeley National Laboratory (LBNL) is gratefully acknowledged. The advise of Dr. Robert Budnitz from LBNL on technical matters is greatly appreciated. The authors thank Brian Terranova of the University at Buffalo, who generated the LS-DYNA results presented in this paper.

References

ASCE, 2005. Seismic design criteria for structures, systems and components in nuclear facilities. ASCE Standard 43, American Society of Civil Engineers, Reston, VA.

ASCE, 2016. Seismic analysis of safety-related nuclear structures and commentary. ASCE/SEI Standard 4, American Society of Civil Engineers, Reston, VA.

Constantinou, M. C., Whittaker, A. S., Kalpakidis, Y., Fenz, D. M., Warn, G. P., 2007. Performance of seismic isolation hardware under service and seismic loading. Tech. Rep. MCEER-07-0012, University at Buffalo, State University of New York, Buffalo, NY.

Fenz, D. M., Constantinou, M. C., 2008. Modeling Triple Friction Pendulum bearings for response-history analysis. Earthquake Spectra 24 (4), 1011–1028.

Gülerce, Z., Abrahamson, N. A., 2011. Site-specific design spectra for vertical ground motion. Earthquake Spectra 27 (4), 1023–1047.

Huang, Y.-N., Whittaker, A. S., Constantinou, M. C., Malushte, S., 2007. Seismic demands on secondary systems in base-isolated nuclear power plants. Earthquake Engineering Structural Dynamics 36 (12), 1741–1761.

Huang, Y.-N., Whittaker, A. S., Kennedy, R. P., Mayes, R. L., 2009. Assessment of base-isolated nuclear structures for design and beyond-design basis earthquake shaking. Tech. Rep. MCEER-09-0008, University at Buffalo, State University of New York, Buffalo, NY.

Huang, Y.-N., Whittaker, A. S., Kennedy, R. P., Mayes, R. L., 2013. Response of base-isolated nuclear structures for design and beyond-design basis earthquake shaking. Earthquake Engineering & Structural Dynamics 42 (3), 339–356.

Huang, Y.-N., Whittaker, A. S., Luco, N., 2010. Seismic performance assessment of base-isolated safety-related nuclear structures. Earthquake Engineering & Structural Dynamics 39 (13), 1421–1442.

Huang, Y.-N., Whittaker, A. S., Luco, N., 2011a. A probabilistic seismic risk assessment procedure for nuclear power plants:(i) methodology. Nuclear Engineering and Design 241 (9), 3996–4003.

Huang, Y.-N., Whittaker, A. S., Luco, N., 2011b. A probabilistic seismic risk assessment procedure for nuclear power plants:(ii) application. Nuclear Engineering and Design 241 (9), 3985–3995.

Kammerer, A., Whittaker, A., Constantinou, M., forthcoming. Technical considerations for seismic isolation of nuclear facilities. Tech. Rep. NUREG-****, United States Nuclear Regulatory Commission, Washington, D.C.

Kumar, M., Whittaker, A. S., Constantinou, M. C., 2015a. Characterizing friction in sliding isolation bearings. Earthquake Engineering & Structural Dynamics 44 (9), 1409–1425.

Kumar, M., Whittaker, A. S., Constantinou, M. C., 2015b. Seismic isolation of nuclear power plants using sliding bearings. Tech. Rep. MCEER-15-0006, University at Buffalo, State University of New York, Buffalo, NY.

Kumar, M., Whittaker, A. S., Kennedy, R. P., Johnson, J. J., Kammerer, A., 2017. Seismic probabilistic risk assessment for seismically isolated safety-related nuclear facilities. Nuclear Engineering and Design 313, 386–400.

LSTC, 2011. LS-DYNA, A program for nonlinear dynamic analysis of structures in three dimensions, v. R5.1.1. Livermore Software Technology Corporation, Livermore, CA.

Mosqueda, G., Whittaker, A. S., Fenves, G. L., 2004. Characterization and modeling of Friction Pendulum bearings subjected to multiple components of excitation. Journal of Structural Engineering 130 (3), 433–442.

PEER, 2014. Open System for Earthquake Engineering Simulation, v. 2.4.3. Pacific Earthquake Engineering Research Center, Berkeley, CA.

Roche, R., 2013. Nuclear power plant testbeds for seismic isolation. Personal Communication to A. Whittaker.

Short, S., Hardy, G., Merz, K., Johnson, J., 2007. Program on technology innovation: validation of CLASSI and SASSI codes to treat seismic wave incoherence in soil-structure interaction (SSI) analysis of nuclear power plant structures. Tech. Rep. 1015111, Electric Power Research Institute, Palo Alto, CA.

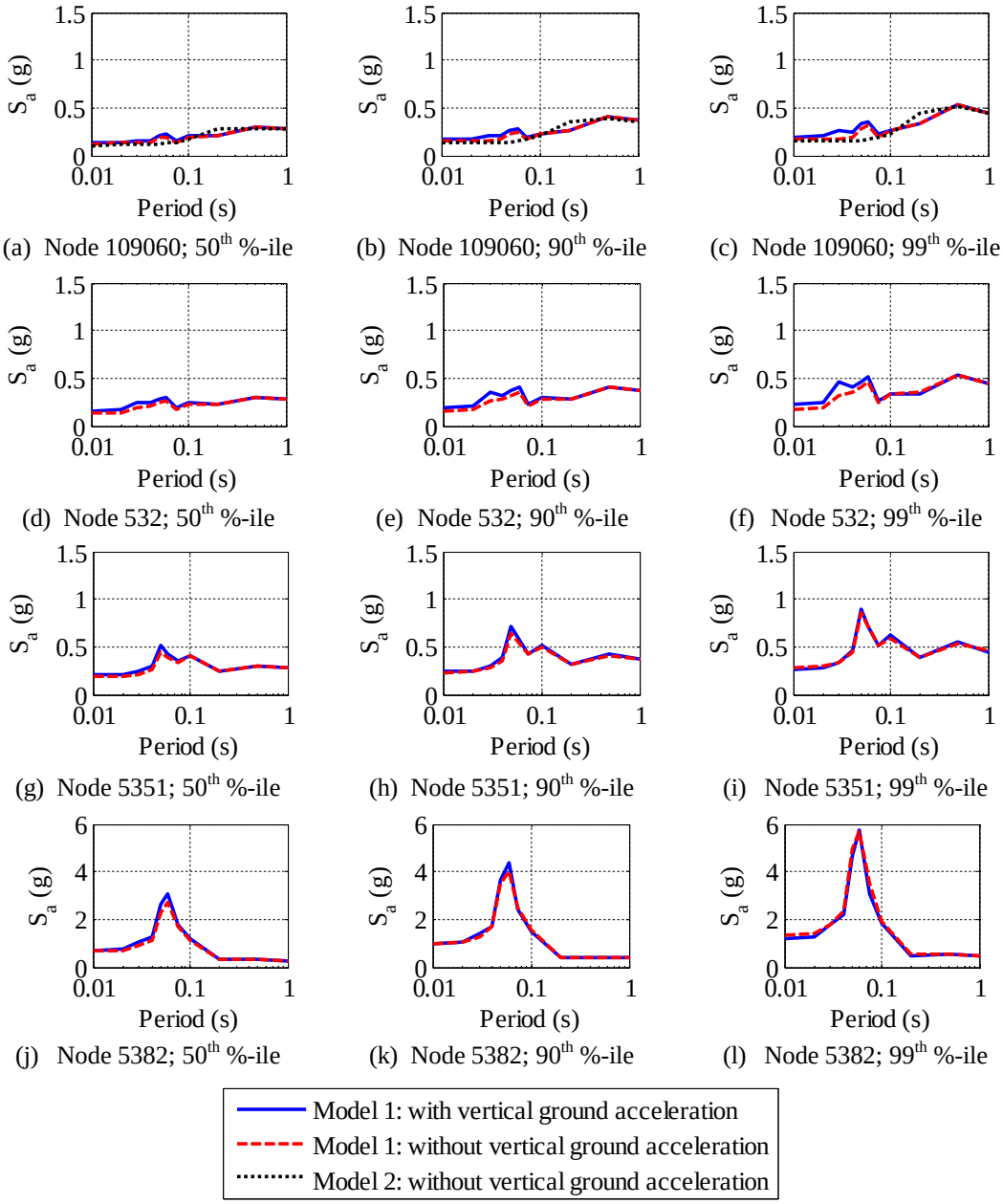

Figure 15: Floor spectra in the X direction at different nodes in the CIS computed using the two NPP models with friction at the sliding surface described using the Coulomb model subjected to the set of 30 ground motions of Figure 10 amplitude scaled by 0.6

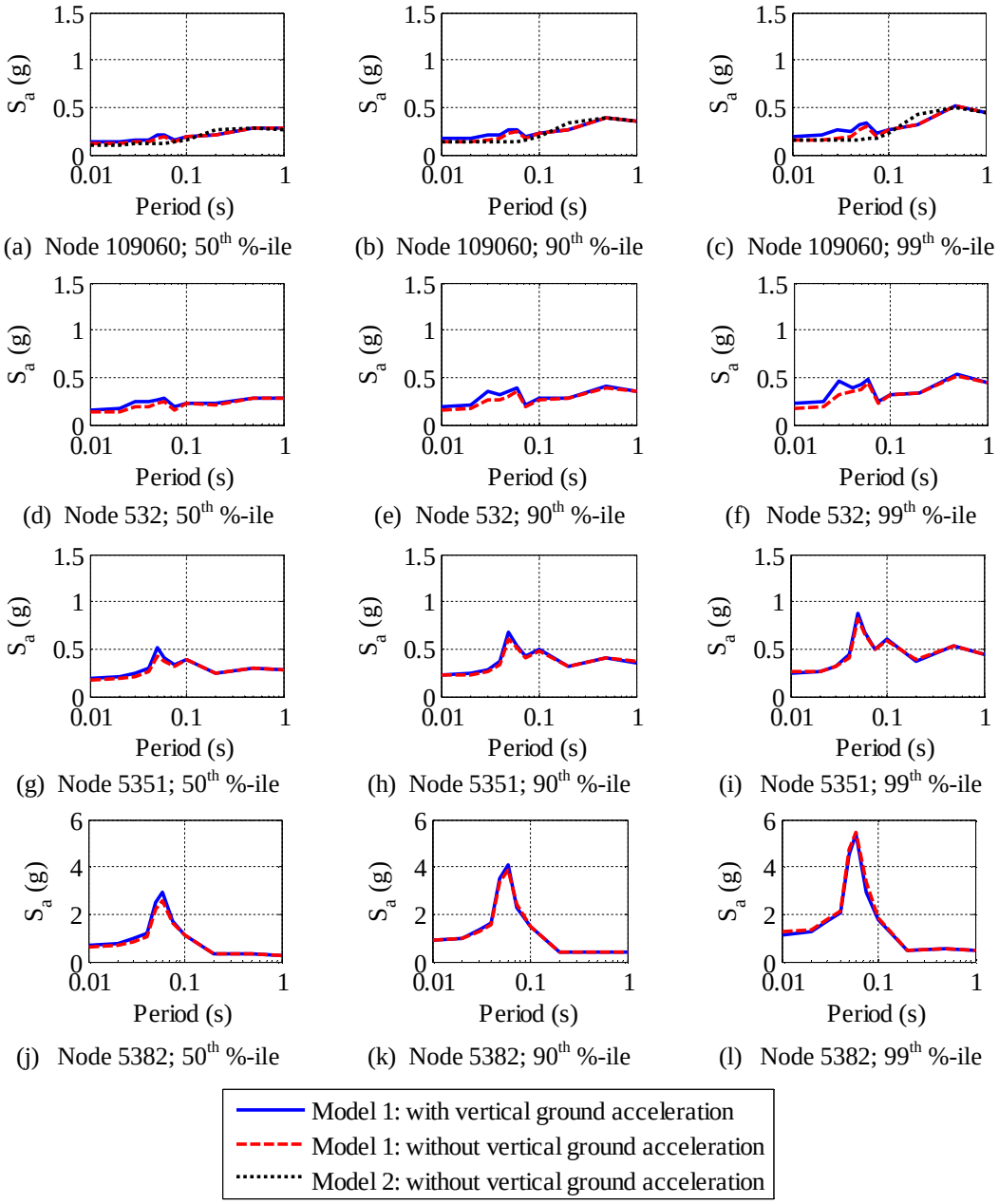

Figure 16: Floor spectra in the X direction at different nodes in the CIS computed using the two NPP models with friction at the sliding surface described using the velocity-dependent model subjected to the set of 30 ground motions of Figure 10 amplitude scaled by 0.6

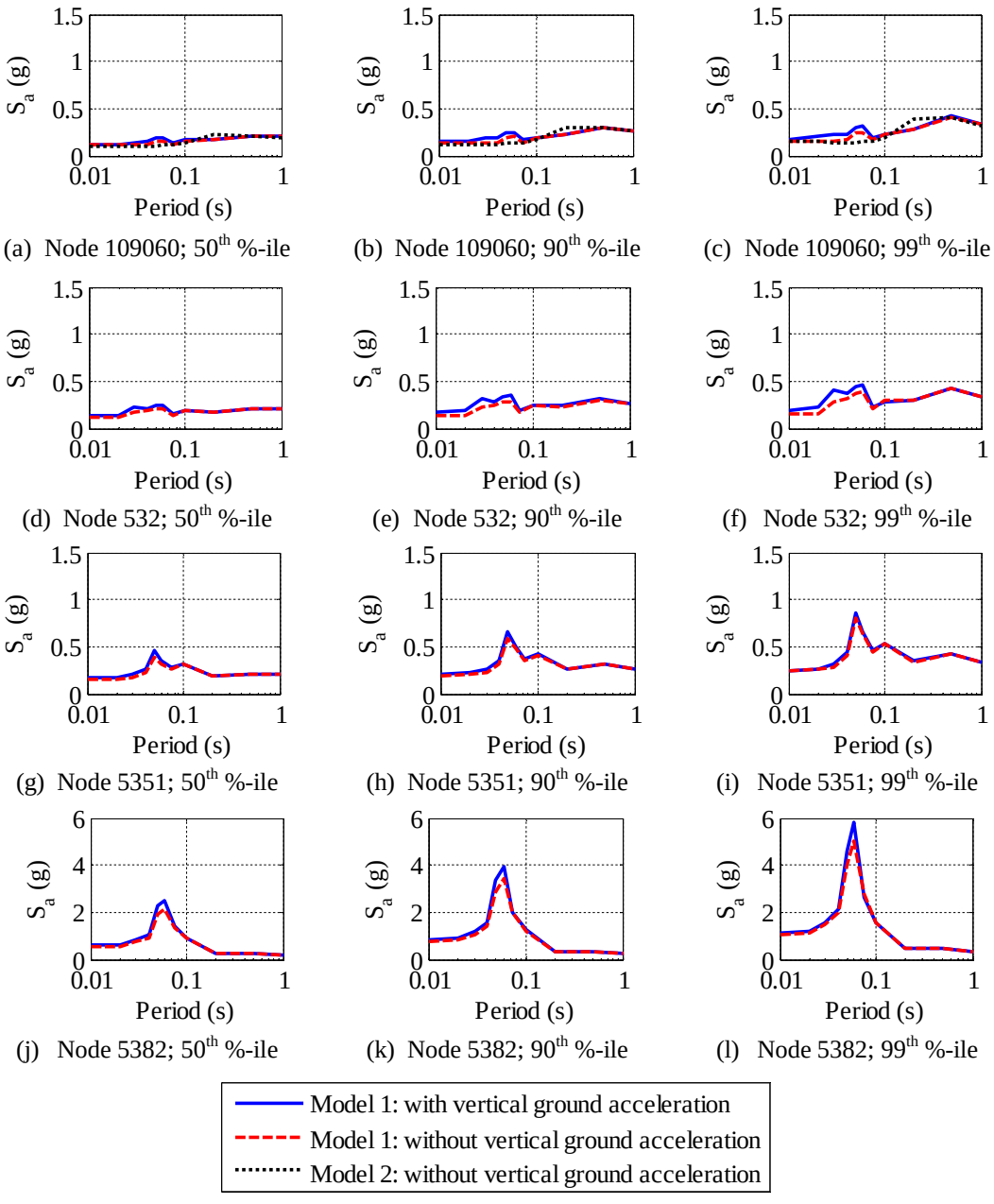

Figure 17: Floor spectra in the X direction at different nodes in the CIS computed using the two NPP models with friction at the sliding surface described using the temperature-dependent model subjected to the set of 30 ground motions of Figure 10 amplitude scaled by 0.6

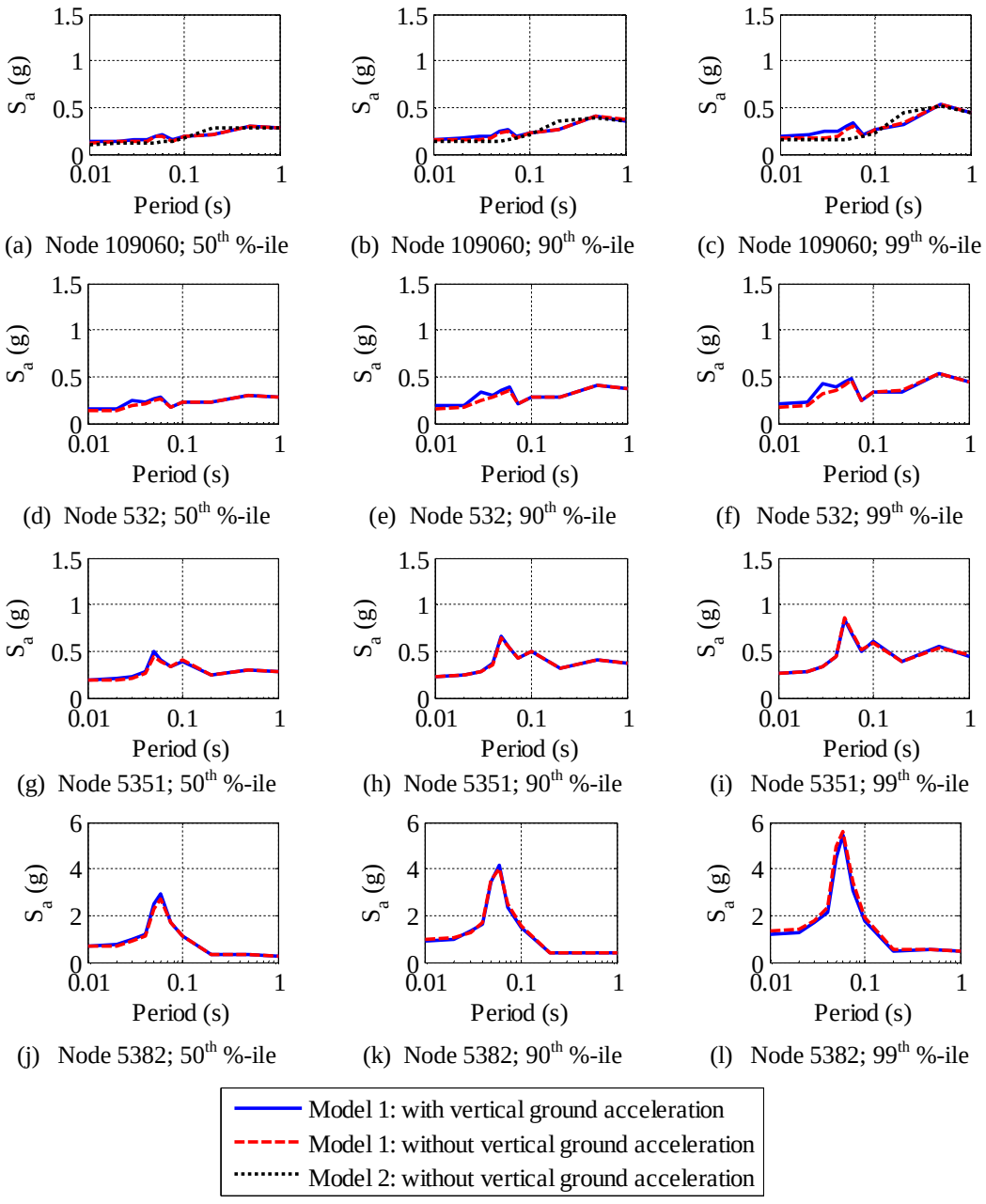

Figure 18: Floor spectra in the X direction at different nodes in the CIS computed using the two NPP models with friction at the sliding surface described using the pressure-dependent model subjected to the set of 30 ground motions of Figure 10 amplitude scaled by 0.6

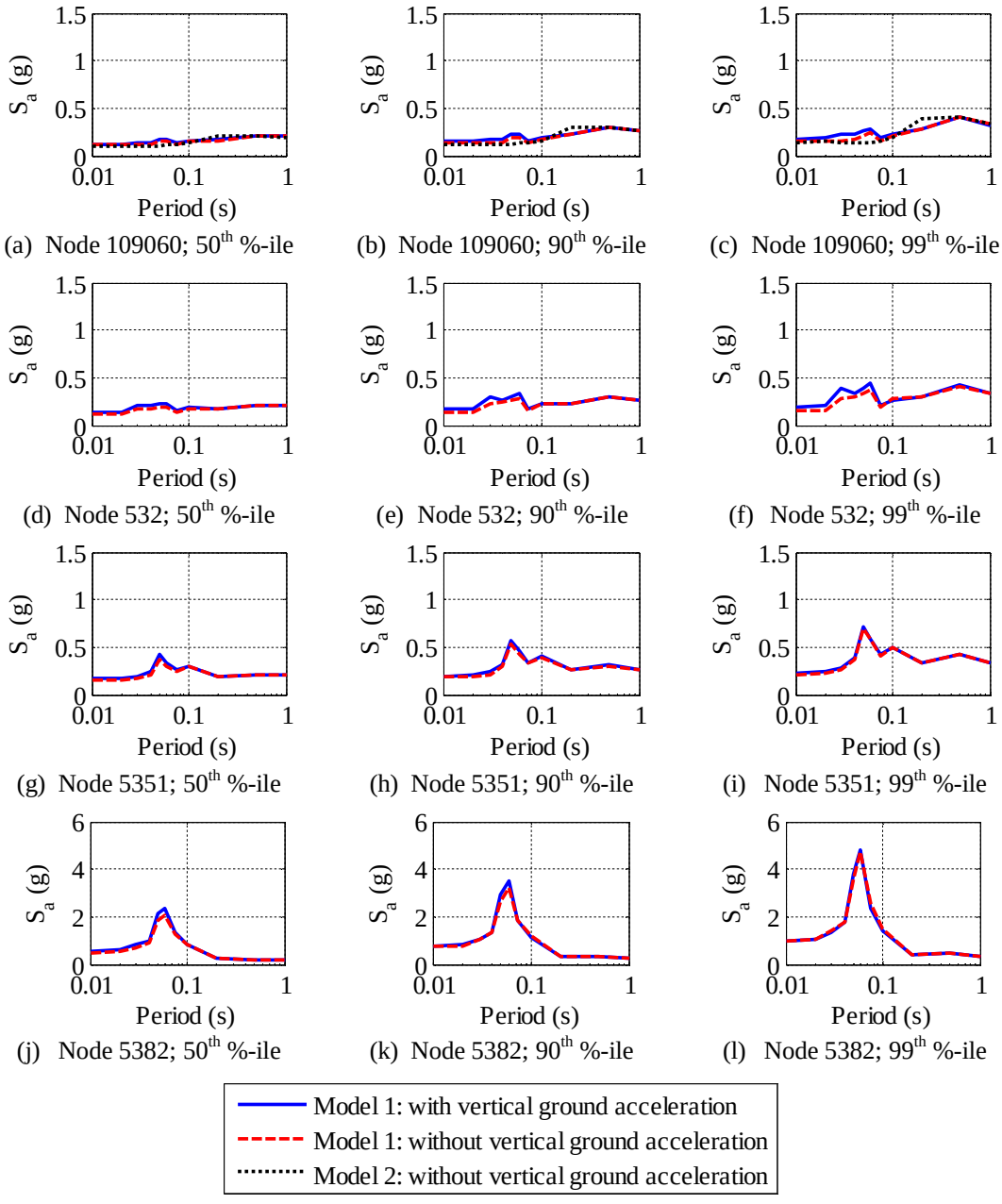

Figure 19: Floor spectra in the X direction at different nodes in the CIS computed using the two NPP models with friction at the sliding surface described using the *p-T-v* model subjected to the set of 30 ground motions of Figure 10 amplitude scaled by 0.6

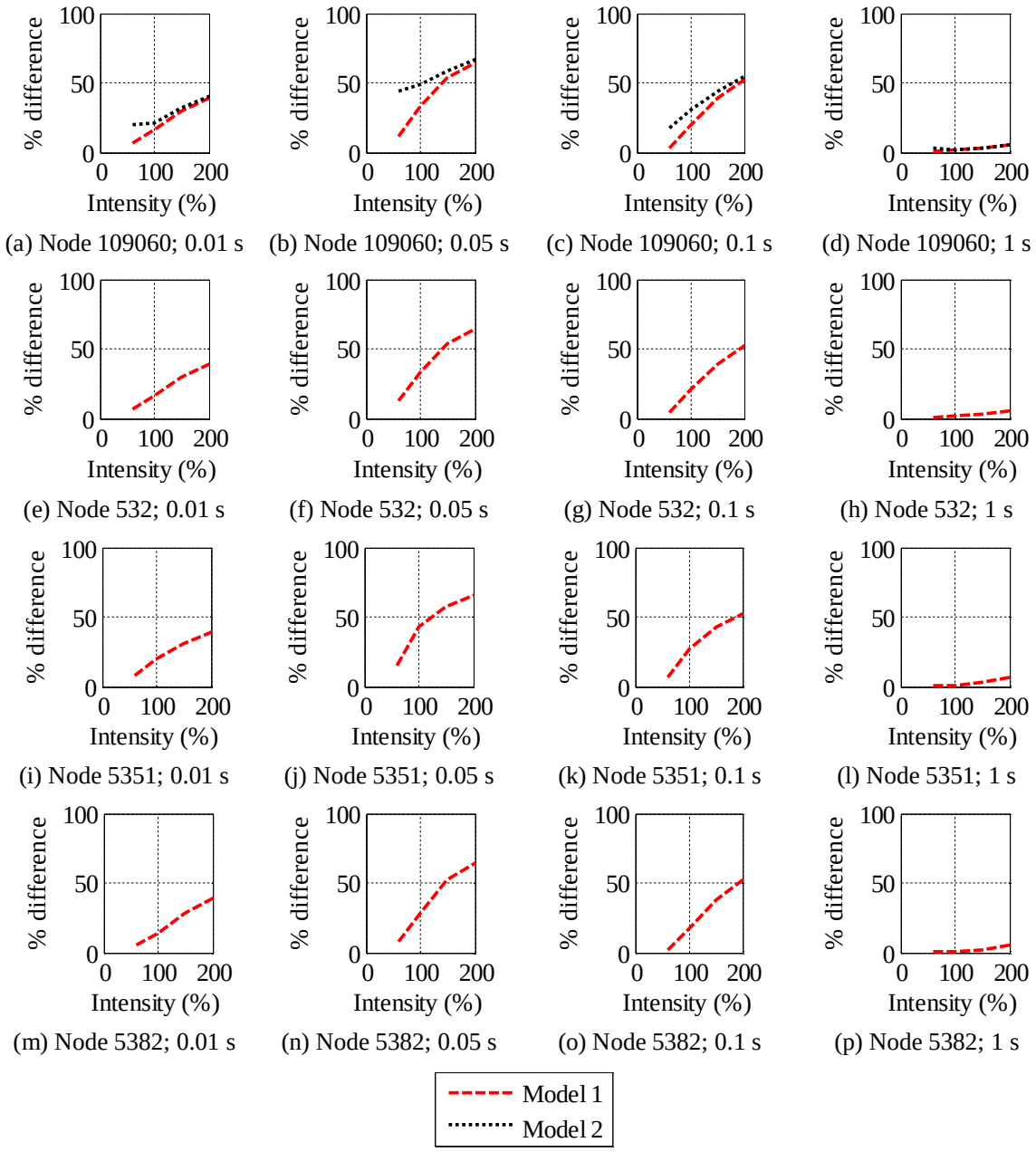

Figure 20: Percentage difference between the median floor spectral ordinates computed using the two NPP models isolated using FP bearings with friction at the sliding surface defined using Coulomb model subjected to two horizontal components of ground motions relative to that computed using Model 1 subjected to three components of the ground motion

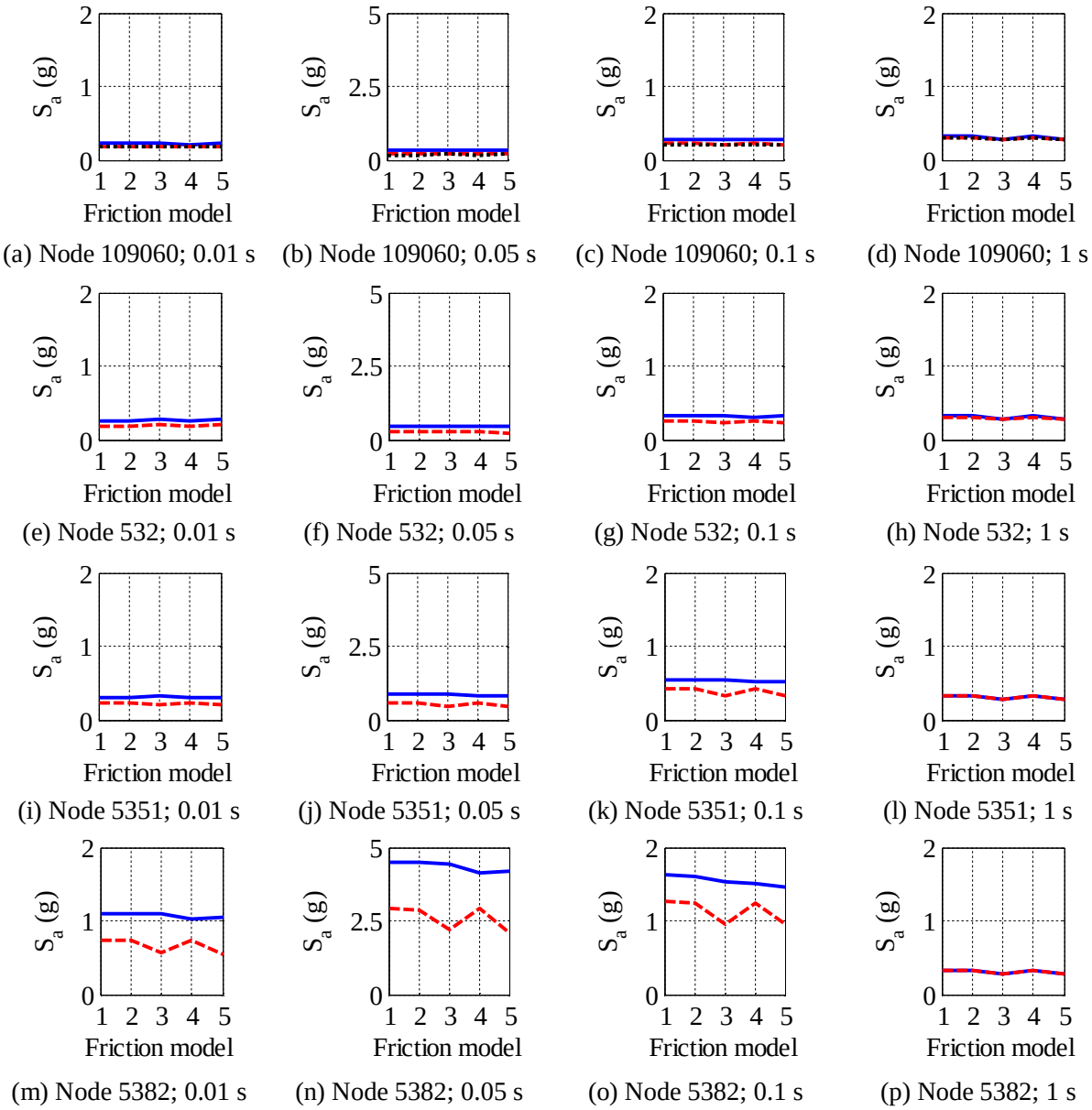

Figure 21: Median spectral accelerations in the X direction for four nodes of the CIS subjected to 30 ground motions of Figure 10 amplitude scaled by 1.0; friction models 1 through 5, respectively, denote Coulomb, pressure-dependent, temperature-dependent, velocity-dependent and *p-T-v* models